Potential description of the positive- and negative-energy properties of the $\alpha + {}^{40}$Ca system and α-cluster structure of ^{44}Ti

F. Michel

Faculté des Sciences, Université de l'Etat, B-7000 Mons, Belgium

G. Reidemeister

Physique Nucléaire Théorique, Université Libre de Bruxelles, B-1050 Bruxelles, Belgium

S. Ohkubo

Department of Applied Science, Kochi Women's University, Kochi 780, Japan

The α-cluster structure of the ^{44}Ti nucleus is investigated within a local potential model description, starting from the unique optical potential which describes elastic ^{40}Ca(α,α) scattering on broad angular and energy ranges, and which has recently been shown to describe the broad oscillations seen in the low energy fusion excitation function as well. It is found that the various α-cluster states group into quasirotational bands whose properties are not dissimilar to those of the well-understood ^{20}Ne nucleus. The lowest lying band is composed of states of even parity with moderate cluster character at low spin; it agrees within a few MeV's in absolute energy with the ^{44}Ti experimental ground state band, and the experimental intraband quadrupole transition probabilities are reproduced with good accuracy. The potential supports an excited positive parity band with strong cluster character, starting a few MeV's above the $\alpha + {}^{40}$Ca threshold; the states of this band with spins ranging from 6 to 12 are responsible for the oscillations observed in the fusion excitation function. It supports, in addition, a negative parity band starting just above the threshold and composed of narrow states with intermediate cluster character; the latter has up to now no experimentally known counterpart. The states of higher lying bands are very broad and overlapping but they play an important role in enhancing the ^{40}Ca(α,α) backward angle cross section. Our results are discussed in terms of the available experimental evidence and of the various, often conflicting theoretical interpretations which have been put forward to describe the ^{44}Ti α-cluster spectroscopy.

I. INTRODUCTION

Whereas the independent particle model has been able to correlate many experimental data throughout the Periodic Table, it is well known that some nuclear levels (the so-called "intruder states") are very difficult to understand within the frame of the shell-model approach, while the detailed properties of some other levels—as their electromagnetic transition rates—can only be described qualitatively. These difficulties, which can be ascribed to the inevitable truncation of the shell-model basis, can in some cases by alleviated by taking into account the underlying cluster structure of these states, which amounts to shifting to a calculational configuration space better adapted to their description. While activity has primarily been focused on relatively light systems, recent developments[1] have revived the interest for α-particle clustering in the lead and actinide regions in connection with the interacting boson model approach to the collective properties of heavy nuclei.

The most fully investigated system within the α-cluster approach is ^{20}Ne, where various rotational bands have been described in terms of $\alpha + {}^{16}$O (g.s.) and $\alpha + {}^{16}$O* cluster states.[2] Not only do the energies E_J of these states follow an approximate $J(J+1)$ behavior, but they are characterized by large α-particle widths and large $B(E2)$ intraband transitions. The best candidates to such a description are the $K^\pi = 0_1^+$ (ground state) and the excited $K^\pi = 0^-$ and 0_4^+ bands, all of which can be viewed as corresponding to an α-particle orbiting an inert ^{16}O core. However in the ground state band there is appreciable overlap between the clusters, and the α-particle character of the states decreases with increasing spin (antistretching effect); its main properties are consistently explained within conventional shell-model approaches, and indeed the α-core relative motion wave functions are found to have substantial overlap with the simple SU(3) wave functions of the leading $(\lambda,\mu) = (8,0)$ representation. In contrast, both the $K^\pi = 0^-$ and 0_4^+ bands consist of states where the rms separation between the clusters is large, and whose reduced α widths are close to the Wigner limit. Their shell-model description would require inclusion of numerous high excitation basis states; they are more economically described in a cluster model basis. In fact, because of the Pauli principle there is a large overlap between these seemingly very different descriptions; in addition, mixing between both types of states is expected to occur. The coexistence and

coupling of both types of structure has been investigated by Tomoda and Arima[3] in a hybrid model space combining ($1s\,0d$)^4 shell-model and $\alpha + ^{16}$O cluster components.

Alpha-particle cluster states have likewise been identified in lower mass systems ranging from ^{16}O to ^{19}F. The importance of α-particle clustering in p-shell nuclei has also been emphasized. For non-alpha nuclei, the interplay between α-cluster states and t- and d-cluster states has to be taken into account.[2,4]

The extension of the α-cluster spectroscopy in the region of the sd-shell closure has met with more limited success. In particular, the structure of ^{44}Ti, which is the analog of ^{20}Ne in the fp shell and is thus of considerable interest, is the matter of contradictory interpretations. The symmetry-breaking effect of the growing spin-orbit interaction on the SU(3) classification has often been invoked to explain why a cluster model description should progressively lose its usefulness in this mass region. Moreover, the relative "softness" of ^{40}Ca as compared with ^{16}O makes it a less favorable candidate for acting as an inert core. On the other hand, the higher level density observed in ^{44}Ti as compared with that of ^{20}Ne makes the experimental identification of α-cluster candidates more intricate.

In this paper we will strive to demonstrate that the present understanding of the α-^{40}Ca interaction which has been extracted from the analysis of the numerous existing ^{40}Ca(α,α) elastic scattering data, and the recent advances made in the interpretation of the oscillations displayed by the $\alpha + ^{40}$Ca fusion excitation function, make possible an unambiguous elucidation of the long-standing problem of the α-particle structure of the ^{44}Ti nucleus. A preliminary account of this work has recently been presented in Ref. 5.

The organization of the paper is as follows. In Sec. II we summarize the experimental situation by enumerating the various ^{44}Ti α-cluster states candidates most often quoted in the literature, and we present the (often conflicting) theoretical interpretations which have emerged from cluster, shell, and hybrid model calculations. Section III is devoted to a discussion of the local potential approach to cluster spectroscopy, with particular emphasis on its relation with the optical model; novel results illustrating the continuity of the two descriptions are presented for the well-understood case of the $\alpha + ^{16}$O system. In Sec. IV we apply the local potential approach to the $\alpha + ^{40}$Ca system, starting from the unique optical potential which has emerged from the analysis of experimental elastic scattering data extending on broad angular and energy ranges. The results of these calculations and their implications for the cluster spectroscopy of ^{44}Ti are discussed in depth in that section, while a summary and our conclusions appear in Sec. V.

of even parity states with spins ranging from 0 to 12, and whose quasirotational appearance is reminiscent of that of ^{20}Ne—a narrow level located at $E_x = 8.54$ MeV, strongly populated in the ^{40}Ca(^{6}Li,d) reaction, which has tentatively been assigned $J^\pi = 0^+$ by Strohbusch et al.,[7] and a narrow ($\Gamma = 40$ keV) $J^\pi = 1^-$ state at $E_x = 11.7$ MeV, which was identified by Frekers et al.[8] by inspection of their ^{40}Ca(α,α_0) excitation function; this state is already clearly visible in the older data of John et al.[9] Broader states with $J^\pi = 0^+$, $E_x = 11.2$ MeV; $J^\pi = 2^+$, $E_x = 12.17$ MeV; and $J^\pi = 3^-$, $E_x = 12.76$ MeV were subsequently extracted from high resolution elastic ^{40}Ca(α,α) data and postulated to form a mixed-parity molecular rotational band together with the $J^\pi = 1^-$, $E_x = 11.7$ MeV state.[10] These various states are presented in Fig. 1(a). [For completeness let us mention two narrow levels[11] with $J^\pi = 2^+$, $E_x = 9.123$ MeV and $J^\pi = 4^+$, $E_x = 9.182$ MeV, strongly excited in ^{40}Ca(α,α) scattering, which have been proposed as band partners of the $J^\pi = (0^+)$, $E_x = 8.54$ MeV state].

On the theoretical side, existing cluster model calculations lead at least to three conflicting interpretations of the ^{44}Ti structure.

Resonating group method (RGM) calculations carried out by Kihara et al.[12] using an adjusted Volkov $V2$ interaction[13] succeeded in reproducing the ground state band structure of ^{44}Ti, including the $B(E2)$ intraband
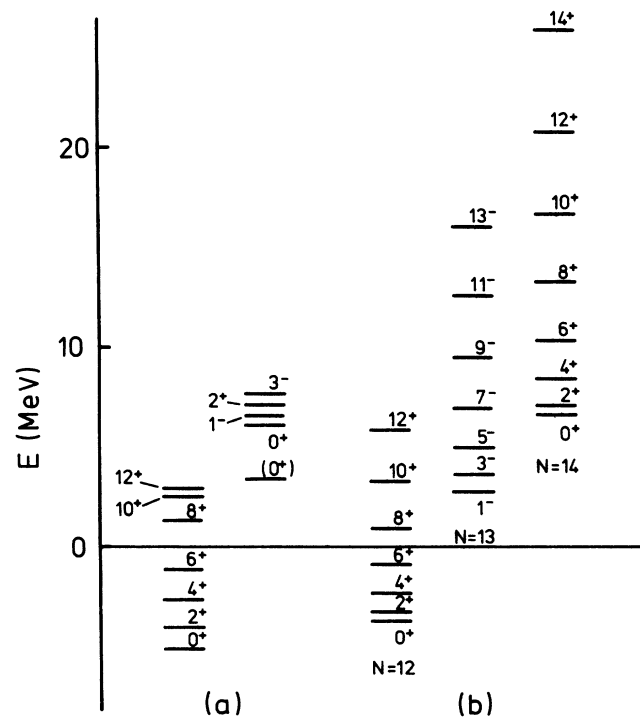

FIG. 1. (a) Experimental ground state band (Ref. 6) and α-particle cluster-state candidates (Refs. 7 and 10) in ^{44}Ti; (b) ^{44}Ti $N = 12$, $N = 13$, and $N = 14$ states supported by the local potential (with $V_0 = 180$ MeV). Energies are given with respect to the $\alpha + ^{40}$Ca threshold.

II. PRESENT STATUS OF THE ^{44}Ti α-CLUSTER SPECTROSCOPY

The states which are most often quoted in connection with the α-cluster spectroscopy of ^{44}Ti are—besides the members of the ground state band[6] which is composed

transitions without having to introduce any additional effective charge. In addition, this calculation predicts another positive parity band whose band head lies near the $J^\pi = (0^+)$, $E_x = 8.54$ MeV state, and an excited negative parity band starting not far from the $J^\pi = 1^-$, $E_x = 11.7$ MeV state. The main difficulty in this picture is that the calculation also locates a low energy negative parity band just above the $\alpha + {}^{40}$Ca threshold, whose members have no known experimental counterparts; also, it fails to reproduce the mixed parity band starting with the $J^\pi = 0^+$, $E_x = 11.2$ MeV state. We note that these features are consistently observed in calculations attempting to reproduce the ground state rotational band of ^{44}Ti.

On the other hand, generator coordinate method (GCM) calculations of the Münster group[14] using the Brink and Boeker $B1$ interaction[15] predict a single band of states with negligible parity splitting, whose low spin members appear at a relatively high excitation energy ($E_x \sim 10$ MeV) and are in good agreement with those of the experimental mixed parity band starting at $E_x = 11.2$ MeV; in these and similar calculations, the ^{44}Ti ground state band is not reproduced and is considered to lie outside the α-cluster model space, and, likewise, the $J^\pi = (0^+)$, $E_x = 8.54$ MeV state has no theoretical counterpart.

Finally, in a recent calculation carried out with an adjusted Volkov $V1$ interaction, Horiuchi[16] predicts a positive parity band whose band head agrees with the $J^\pi = (0^+)$, $E_x = 8.54$ MeV state, and a negative parity band starting at an energy compatible with that of the $J^\pi = 1^-$, $E_x = 11.7$ MeV state; here also the ^{44}Ti ground state band is not reproduced, nor are the $J^\pi = 0^+$, 2^+ experimental levels thought to be the band partners of the $J^\pi = 1^-$, $E_x = 11.7$ MeV state.

Shell-model calculations[17] have also been reported for this system; as they generally suppose an inert ^{40}Ca core and limit the active space to the fp shell, their predictions are restricted to positive parity states. They give a satisfactory account of the ground state band properties, although detailed agreement with experiment is lacking for the energy spacings of the low spin members of the band, and large effective charges ($\delta e \sim 0.5$ e) have to be introduced to reproduce the intraband $B(E2)$ experimental values. Subsequent calculations showed that it is possible to remedy these defects by supplementing the $(fp)^4$ shell-model basis with $\alpha + {}^{40}$Ca cluster components.[18] Examination of the calculated wave functions reveals a non-negligible admixture of cluster components for the low spin members of the g.s. band, which is instrumental to the reproduction of the intraband $B(E2)$'s with more reasonable effective charges; it is to be noted that the explicit consideration by Arima and Tomoda[19] of the influence of spin-orbit coupling showed that its presence is not incompatible with a sizable α-cluster component in the ^{44}Ti ground state band, although comparison with similar calculations by the same authors[3] of the ^{20}Ne properties shows that the ^{44}Ti states are more shell-model-like than the latter. In addition, the same calculations produce excited rotational bands with a stronger cluster character: the most elaborate calcula-

tion, performed by Itonaga,[18] predicts two negative parity bands and an excited positive parity band in essential agreement with those disclosed by the RGM calculation of Kihara et al.[12]

III. THE LOCAL POTENTIAL MODEL APPROACH

A more phenomenological but powerful approach to the description of cluster structure in nuclei was initiated some ten years ago by Buck et al.:[20] they showed that simple deep local intercluster potentials, similar to those generated by folding model calculations, are capable of reproducing—often with remarkable accuracy—many properties of cluster states such as their energy spacings, α-particle widths, and electromagnetic properties.

A direct support has recently been given to this approach by Horiuchi,[21] who succeeded, by relying on the semiclassical approximation, in deriving from the complicated intercluster RGM nonlocal kernels effective local equivalent potentials, to be used in a relative motion one-body Schrödinger equation, and giving phase shifts close to those derived in the complete microscopic calculation; these potentials generally display mild energy and angular momentum dependence. Mention should also be made of the alternative methods of Friedrich et al.,[22] which derive the intercluster potential from the microscopic intrinsic or angular momentum projected energy surfaces of the GCM, and lead to an energy-independent (but possibly l-dependent) interaction, and of the fixed-energy inverse scattering methods used by Baldock et al.[23] and by Lipperheide et al.,[24] which lead to an l-independent, slowly energy-dependent nucleus-nucleus potential. Whatever the particular method used, however, all these potentials are deep, since they have to accommodate a number of bound states corresponding to that of the forbidden states of the RGM.[25]

The local potential description of α- and t-cluster states has been successfully applied to many nuclei of the p and of the sd shell.[20] In particular, the model has been highly successful in accounting for the detailed properties of the $K^\pi = 0_1^+$ and 0^- α-cluster bands in ^{20}Ne, as the level energy spacings, the α-particle widths, and the ground state band electromagnetic transition rates using only a small renormalization of the effective charge.

There have been fewer applications of the local potential model in the sd-shell closure region; to our knowledge calculations have thus far been limited to the ^{40}Ca, ^{43}Sc, and ^{44}Ti systems.[26-28] As, in the ^{44}Ti case, the calculations have been restricted to states of the ground state band,[26,27] they shed no light on the identification of higher energy α-cluster states in that system. However, it is interesting to note that some of the intercluster local potentials built by Pal and Lovas[27] give a fair account of the energies of the low spin members of the ^{44}Ti ground state band and of the excited 4p-4h band in ^{40}Ca based on the $J^\pi = 0^+$, $E_x = 3.35$ MeV state, which in a weak coupling picture should have closely similar properties; moreover the calculated intraband quadrupole transition probabilities between these states were found to be in satisfactory agreement with the available experimental data, without having to

introduce any effective charge. More recently, Merchant[28] has investigated within the frame of the same model the case of the ^{43}Sc nucleus, which is the fp-shell analog of ^{19}F, and whose α-particle states should, therefore, in a weak coupling picture be related to those of ^{44}Ti as the α-particle states of ^{19}F are related to those of ^{20}Ne. Although the problem is complicated by the nonzero spin of the ^{39}K core, a good description of the energy location of the low-lying positive parity states of ^{43}Sc and of the enhanced $B(E2)$'s between these states was obtained in that work.

Despite its success in accounting for many detailed properties of the ^{44}Ti ground state band, the local potential model does not allow us to decide in an unambiguous way which of the $\alpha + {}^{40}$Ca cluster model calculations summarized above provides the most physically satisfying picture. Indeed it is unable—because of its essentially phenomenological nature—to predict *absolute energies* with respect to the threshold, and its precise depth is usually fixed by reference to some set of well established cluster levels of the unified system. The local potential should, however, share with the more complicated microscopic interaction it is supposed to represent the property to describe in a unified way the bound, quasibound, and scattering properties of the system under investigation; therefore, it is expected to bear a close connection with the optical model potential describing low energy α-particle scattering from the core nucleus.

This condition is unfortunately of little help in most cases of practical interest since the empirical nucleus-nucleus optical potentials deduced from experiment are known to suffer from various ambiguities, in particular at low energies where strong absorption usually dominates the scattering. An exception to this general behavior is, however, supplied by the $\alpha + {}^{16}$O and $\alpha + {}^{40}$Ca systems, where the closed-shell nature of the targets makes the absorption substantially weaker than for most neighboring systems, causing a spectacular enhancement of the low energy elastic cross sections at large angles (the so-called ALAS phenomenon).[29,30] This exceptional transparency made possible an unambiguous determination of the underlying potential, the discrete ambiguity being lifted by extending the analysis to high energy data satisfying the Goldberg's criteria.[31]

The case of the $\alpha + {}^{16}$O optical potential is a very important one to investigate in order to test the above ideas. In fact, extrapolation towards low energies of the real part of the unique optical potential of Ref. 30 provides an excellent description of the $K^{\pi}=0_1^+$, 0^-, and 0_4^+ rotational bands in ^{20}Ne. In particular, it automatically locates the ground state band—that is, the one composed of states with $N \equiv 2n_r + l = 8$, where n_r denotes the number of radial nodes of the wave function—within a few MeV's of its experimental counterparts; states with $N < 8$ are discarded since they correspond to the states forbidden by the Pauli principle in a cluster model approach. Moreover, the same potential predicts electromagnetic properties and α-particle widths for these states in remarkable agreement with experiment. As an example we list in Table I the electromagnetic $B(E2)$ transition probabilities within the

TABLE I. Comparison of the calculated intraband quadrupole transition probabilities within the $N=8$ and $N=9$ ^{20}Ne bands with the experimental data (an effective charge $e_{\mathrm{eff}}=1.05$ e has been used for the $N=8$ transitions, see text), and of the calculated widths within the $N=9$ band with their experimental counterparts.

J^{π}	$B(E2)$ $(J \rightarrow J-2)$ $(e^2\,\mathrm{fm}^4)$	
	This work	Expt. (Ref. 32)
0^+		
2^+	53	65±3
4^+	71	71±6
6^+	66	64±10
8^+	32	29±4
1^-		
3^-	141	161±26
5^-	158	

J^{π}	Γ (keV)	
	This work	Expt. (Ref. 32)
1^-	40×10^{-3}	$(28\pm3)\times10^{-3}$
3^-	12	8.1±0.3
5^-	170	145±40
7^-	580	380

^{20}Ne ground state and first negative parity bands; the calculations were carried out using the real part of the potential of Ref. 30, after finely tuning the parameter (denoted as α) controlling its depth in order to locate each state at the correct experimental energy. [For states located above the threshold the calculation was carried out in the bound state approximation. This provides results nearly independent of the exact way the approximation is implemented provided the state is located well below its barrier. For states nearer to the barrier top, which correspond to broader resonances, the calculated $B(E2)$'s are more sensitive to the details of the calculation, and the corresponding experimental measurements are extremely difficult; therefore, we have restricted the calculation for the $K^{\pi}=0^-$ band to the $3^- \rightarrow 1^-$ and $5^- \rightarrow 3^-$ transitions.] A very small renormalization of the bare electron charge was needed in order to bring the absolute $B(E2)$'s in agreement with the ground state band data: use was made of an effective charge $e_{\mathrm{eff}}=1.05$ e, which as can be seen from inspection of Table I brings the theoretical values within a few percent of their experimental counterparts.[32] For the first negative parity band no effective charge was introduced in the calculation, since the experimental data are restricted to the 3^- $(E_x=7.156$ MeV$) \rightarrow 1^-$ $(E_x=5.785$ MeV$)$ transition;[33] because of the stronger α-cluster character of the $K^{\pi}=0^-$ band, the predicted intraband $B(E2)$'s are seen to be considerably enhanced with respect to those of the g.s. band, and indeed the only experimental result is seen to be in very gratifying agreement with that prediction. We have likewise calculated the α-particle widths of the members of the $K^{\pi}=0^-$ band from the energy variation of the corresponding phase shifts, as $\Gamma_l = 2/(d\delta_l/dE)$ at the energy where δ_l passes $\pi/2$. Although the calculated widths are some 1.2 to 1.5 times too large with

respect to experiment (Table I), our simple model gives an excellent account of the enormous 15 000-fold increase of the widths spanned by the data.

We defer a more complete discussion of the low energy properties of the $\alpha + {}^{16}O$ system to a forthcoming publication; the results presented here suffice, however, to demonstrate the virtues of an extrapolation towards low and negative energies of the optical potential used to describe the scattering properties of the system at higher energy. They show in particular that the use of simple local, l-independent, weakly energy-dependent empirical potentials is not restricted—contrary to what has sometimes been claimed[14]—to incident energies above the Coulomb barrier. It is to be noted in this respect that a very recent microscopic calculation by Wada and Horiuchi[34] has confirmed the main properties of the real part of the $\alpha + {}^{16}O$ empirical potential of Ref. 30 in a wide energy range. For the nucleon-nucleus system the merits of such a unified description of bound state and scattering properties has been recognized for a long time.[35] The link between the optical and the shell-model potentials has very recently been investigated by Mahaux and Sartor[36] in the case of nucleon scattering within a dispersion relation approach; although the energy dependence of the transition is not necessarily simple, these calculations indicate that it is a continuous one, and that it can be represented by a relatively small readjustment of the parameters of the real part of the optical model potential used at positive energy.

IV. THE $\alpha + {}^{40}Ca$ OPTICAL POTENTIAL AND α-CLUSTER SPECTROSCOPY OF ${}^{44}Ti$

The $\alpha + {}^{40}Ca$ system has focused considerable experimental and theoretical interest in connection with the spectacular backward angle enhancement seen at low energy in the elastic scattering cross sections. Although there was much speculation at one time on the possible origin of the ALAS phenomenon, there is now general agreement that the only anomalous feature of the system is its particularly low absorption,[29,37−40] which is due in all likelihood to the closed-shell nature of the partners. This anomaly could—as was the case for the $\alpha + {}^{16}O$ system, see above—be turned to an advantage, as it has allowed a precise determination of the underlying optical potential on a wide energy range.[29,40] Although comparison with experiment is complicated at low energy by the occurrence of Ericson fluctuations and compound elastic scattering, it has recently been shown in Ref. 41 that the global potential originally extracted by Delbar et al.[29] for energies ranging from $E_\alpha = 24$ to 166 MeV could be successfully extrapolated down to at least 12 MeV incident energy, and that good agreement could even be obtained with the very low energy ($E_\alpha = 5.0$ to 12.5 MeV) excitation functions of John et al.[9]

The real part of this global potential, which will consistently be used in the following, is of Woods-Saxon squared type:

$$V(r) = -V_0 \{ 1 + \exp[(r-R)/a] \}^{-2} \qquad (4.1)$$

with $R = 4.685$ fm and $a = 1.290$ fm. It is supplemented

with the Coulomb potential due to a uniformly charged sphere of radius $R_c = 4.446$ fm. The energy behavior of V_0 (which is the only energy-dependent parameter for the real part) found adequate to represent the evolution of the data between 24 and 166 MeV is

$$V_0 = 198.6(1 - 0.00168E_\alpha) \text{ MeV} . \qquad (4.2)$$

However, this prescription does not prove entirely satisfactory at the low energy end of this range, since it leads to volume integrals per nucleon pair $J_v/4A$ of some 370 MeV fm^3, while model-independent analyses of the same data[39,40] point to a value lower by approximately 20 MeV fm^3, which corresponds, if the effect is ascribed to a decrease of the potential depth, to $U_0 \cong 180$ MeV. This reduction is not to be considered as an arbitrary manipulation, since two effects have recently been described which both result in a saturation of the real potential depth at low energy. The first one is the energy dependence which emerges when localizing the nonlocal RGM interaction; this effect has been thoroughly investigated by Aoki and Horiuchi[42] in the case of the $X + {}^{16}O$ systems, where X denotes any light-ion projectile with $A \leq 4$. The second effect is due to a dispersion correction to the real potential connected with the rapid opening of nonelastic channels above the threshold; it has been studied in detail by Mahaux et al.[43] for the $\alpha + {}^{16}O$ and $\alpha + {}^{40}Ca$ systems. As their magnitude and localization in energy are rather similar, these two effects will probably be difficult to disentangle in concrete cases. We note that the changes they induce in the potential are not restricted to a simple renormalization of the depth; however, for the sake of simplicity and in view of the uncertainties which affect both the theoretical estimates and the empirical potential itself, we will content ourselves in the following of tuning the V_0 parameter when required.

A. The ${}^{44}Ti$ ground state band

In the case of the $\alpha + {}^{40}Ca$ system, states with $N \equiv 2n_r + l < 12$ correspond to states of the RGM forbidden by the Pauli principle, and they should therefore be discarded. The first states susceptible of physical interpretation are those with $N = 12$. We have calculated their energy location using the real part of various low-energy potentials belonging to the unique potential family fitting the higher energy data, including the global potential discussed above; the energy of the states located above the threshold, which are found to lie well below their respective effective potential barriers, was calculated in the bound state approximation. Quite remarkably, these states are found to group into a quasirotational band (with even spins ranging from 0 to 12), whose band head falls within a few MeV's from the ${}^{44}Ti$ ground state.[44] Moreover, the average energy spacing is found to be compatible with that of the ${}^{44}Ti$ ground state band, although the spacing between the 0^+ and 2^+ states tends to be smaller than experiment, and the calculation fails to reproduce the collapse observed at the high energy end of the band (it has to be remarked in this respect that, as has also been emphasized by Pal and Lovas,[27]

the local potential built by Pilt[26] to mock up this collapse is a highly artificial one, in that its geometry and depth are totally incompatible with those of potentials fitting the low energy scattering data).

A comparison of the ^{44}Ti experimental ground state band with the states of the $N = 12$ band, calculated using the potentials derived by Gubler et al.[40] from an extensive analysis of their very detailed experimental angular distributions, is presented in Fig. 2. The latter have a Woods-Saxon raised to the fifth power form factor; only the potentials deduced from data extending on the whole angular range, which are determined with the best accuracy, were retained in our calculation. Although their parameters were determined independently at each energy, all these potentials lead to remarkably similar results. In particular, the $N = 12$ band head is located at about 6 to 9 MeV below the threshold, that is, 1–4 MeV below the ^{44}Ti ground state, confirming the need for a slight reduction of the potential depth when energy decreases. We also show in Fig. 2 the location of the states calculated with the global potential of Eq. (4.1), where the depth V_0 was fixed to the value $V_0 = 180$ MeV (which corresponds to a volume integral $J_v/4A$ of 350 MeV fm^3); this value is seen to locate correctly the intermediate part of the spectrum, which on the whole appears to be somewhat too compressed with respect to experiment.

To investigate further the capabilities of the local potential description of the ^{44}Ti ground state band, we calculated the intraband quadrupole transition probabilities and rms intercluster separations from the model wave functions. Here and in the following, use was made of the global potential of Eq. (4.1), whose depth V_0 was finely tuned to locate each state at the correct experimental energy. Values derived for the $B(E2)$'s and rms radii are presented in Table II, together with the depths V_0 needed for each state and the experimental transition probabilities.[45] It can be seen that the latter are nicely reproduced by the calculation without having to introduce any effective charge, whereas large effective charges are required in $(fp)^4$ shell-model calculations to reproduce the data. For illustration we also list in Table II the $B(E2)$ values obtained by Itonaga[18] in a pure shell-
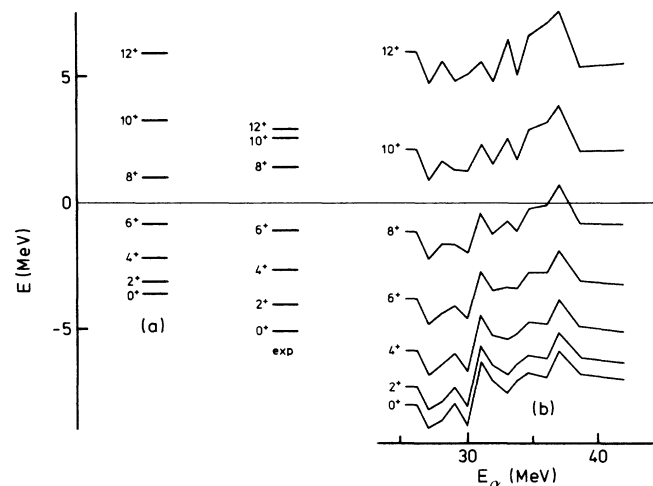

FIG. 2. Comparison of the ^{44}Ti experimental ground state band with (a) the $N = 12$ states supported by our local potential with $V_0 = 180$ MeV and (b) the $N = 12$ states supported by the real part of the various Woods-Saxon raised to the fifth power $\alpha + ^{40}$Ca optical potentials of Gubler et al. (Ref. 40).

model calculation, and the values he obtains when his configuration space is enlarged by introducing additional α-cluster components. It is seen that mixing of the latter into the shell-model components alleviates the initial discrepancy, although the values obtained are still too low with respect to experiment (and to those obtained in our calculation).

On the other hand, the rms intercluster distance is seen to decrease from 4.50 to 3.83 fm when going from the 0^+ to the 12^+ member of the band. As the sum of the radii of the free clusters amounts to 5.16 fm,[46] the overlap between the clusters, which is already significant at low spin, thus becomes severe for the last members of the band; this antistretching effect makes the cluster character of these states much weaker than that observed at low spin, as will be confirmed more quantitatively below, and in accordance with the findings of Itonaga.[18] We note in passing that the result we obtain for the ground state agrees well with the charge radius de-

TABLE II. Calculated rms radii and quadrupole transition probabilities for the states of the ^{44}Ti $N = 12$ band; the second column lists the depths V_0 used to locate each state at the experimental energy of its ^{44}Ti ground state band counterpart. The theoretical $B(E2)$'s are compared with the experimental data (Ref. 45) and with the shell-model and shell-model plus cluster calculations of Itonaga (Ref. 18).

J^π	V_0 (MeV)	$\langle R^2 \rangle^{1/2}$ (fm)	Expt.	$B(E)$ $(J \to J - 2)$ $(e^2 \text{fm}^4)$ This work	Shell model	Shell model plus cluster
0^+	184.1	4.50				
2^+	182.5	4.51	120±30	107.3	40.0	83.8
4^+	181.2	4.47	280±60	146.4	53.4	111.6
6^+	180.7	4.38	160±20	140.2	51.6	105.0
8^+	179.0	4.27	>14	118.1	44.0	77.9
10^+	181.8	4.06	140±30	74.9	32.0	47.4
12^+	186.8	3.83	40±8	33.6	17.3	16.8

duced from the analysis of electron scattering and muonic x-ray data, which unfortunately are only available for ^{nat}Ti. Indeed the rms charge radius corresponding to an intercluster rms distance $\langle R^2 \rangle^{1/2}$ is given by

$$\langle r^2 \rangle_{ch} = \tfrac{10}{121} \langle R^2 \rangle + \tfrac{1}{11} \langle r^2 \rangle_\alpha + \tfrac{10}{11} \langle r^2 \rangle_{Ca} , \qquad (4.3)$$

where $\langle r^2 \rangle_\alpha^{1/2}$ and $\langle r^2 \rangle_{Ca}^{1/2}$ denote the α-particle and ^{40}Ca rms charge radii. Taking the values $\langle r^2 \rangle_\alpha^{1/2} = 1.674$ fm and $\langle r^2 \rangle_{Ca}^{1/2} = 3.48$ fm,[46] together with $\langle R^2 \rangle^{1/2} = 4.50$ fm, we find $\langle r^2 \rangle_{ch}^{1/2} = 3.597$ fm, to be compared with the experimental value $\langle r^2 \rangle_{ch}^{1/2} = 3.60$ fm.[46]

Before we embark upon a closer inspection of our relative motion wave functions, it is useful to comment on the link of the local potential wave functions with those supplied by the microscopic approaches. Our wave functions, which will hereafter be referred to as $u_l(r)$, are supposed to mimic orthogonality condition model (OCM) -type wave functions. As has been emphasized by Buck, Friedrich, and Wheatley,[20] the most justified interpretation of the OCM equation[47]

$$\Lambda_l (T + V - E) \Lambda_l \phi_l = 0 \qquad (4.4)$$

is that it provides a relative motion wave function which is a good approximation to the exact RGM wave function χ_l through the relation

$$\phi_l = (1 - K_l)^{1/2} \chi_l , \qquad (4.5)$$

where K_l stands for the RGM overlap kernel; in an harmonic oscillator (HO) description where the cluster wave functions are represented as Slater determinants with a common HO parameter $\nu = m\omega/2\hbar$, the eigenstates of $(1 - K_l)$ are known to be HO wave functions $u_{Nl}^{HO}(r)$ with HO parameter $\nu' = \mu\nu$, where μ denotes the reduced mass number of the system. Denoting the corresponding eigenvalues by μ_N we thus have the spectral decomposition

$$1 - K_l = \sum_N \mu_N | u_{Nl}^{HO} \rangle \langle u_{Nl}^{HO} | . \qquad (4.6)$$

The eigenvalues of $(1 - K_l)$ are expressible in closed form; in the case of the $\alpha + {}^{40}$Ca system they are given by[48]

$$\mu_N = \sum_{k=0}^{4} (-1)^k \begin{bmatrix} 4 \\ k \end{bmatrix} \sum_{r=0}^{k} \begin{bmatrix} k \\ r \end{bmatrix} 2^{r-k} (\tfrac{11}{40})^{2(k-r)} \sum_{p=0}^{r} \begin{bmatrix} r \\ p \end{bmatrix} (\tfrac{11}{40})^p \Theta(N - p - 2k + 2r) \frac{N!}{(N-p-2k+2r)!} (1 - \tfrac{11}{40}k)^{N-p-2k+2r} . \qquad (4.7)$$

The first eigenvalues are equal to zero; they correspond to the exactly forbidden states of the RGM, which are HO wave functions $| u_{Nl}^{HO} \rangle$ with $N < 12$. The operator Λ_l of Eq. (4.4), which projects out these states, is thus written

$$\Lambda_l = 1 - \sum_{N<12} | u_{Nl}^{HO} \rangle \langle u_{Nl}^{HO} | . \qquad (4.8)$$

It is interesting for estimating the cluster properties of the physical states to evaluate the reduced width amplitude y_l,[49] which is defined in terms of the RGM wave function χ_l by

$$y_l = (1 - K_l) \chi_l , \qquad (4.9)$$

or, taking Eq. (4.5) into account

$$y_l = (1 - K_l)^{1/2} \phi_l ; \qquad (4.10)$$

the associated spectroscopic factor S_α is written

$$S_\alpha = \int_0^\infty dr\, y_l^2(r) . \qquad (4.11)$$

Expanding the relative motion wave function of Eq. (4.5) in the HO basis,

$$\phi_l(r) = \sum_N c_{Nl} u_{Nl}^{HO}(r) \qquad (4.12)$$

makes possible the calculation of the reduced width amplitude and spectroscopic factor in terms of these expansion coefficients and the overlap kernel eigenvalues according to

$$y_l(r) = \sum_N (\mu_N)^{1/2} c_{Nl} u_{Nl}^{HO}(r) , \qquad (4.13)$$

$$S_\alpha = \sum_N \mu_N c_{Nl}^2 . \qquad (4.14)$$

Although the evaluation of these quantities can, strictly speaking, only be performed within the frame of an HO description, it is reasonable to extend this formalism to our local potential wave functions $u_l(r)$. Indeed, the latter are directly comparable to the OCM wave functions $\phi_l(r)$, and they are automatically orthogonal to the deeply bound states supported by the potential, which simulate the RGM forbidden states and turn out to be very similar to HO wave functions provided a choice is made of a convenient HO parameter. The often used prescription $\hbar\omega = 41 A^{-1/3}$ MeV, which leads to an oscillator parameter $\nu \simeq 0.14$ fm^{-2}, fulfills this requirement with excellent accuracy, especially for the most deeply bound of these states. For example, the overlaps of the six $J^\pi = 0^+$ unphysical states supported by potential (4.1), using $V_0 = 180$ MeV, with HO states $(\nu' = \mu\nu = 0.509$ fm$^{-2})$ with $(N,l) = (0,0)$ to $(10,0)$, range from 0.999 to 0.936, and the overlap of the only spurious $J^\pi = 10^+$ state with the $(N,l) = (10,10)$ HO wave function is 0.994.

We have expanded the local potential wave functions of the states of the $N = 12$ band in the HO basis with $\nu' = 0.509$ fm^{-2}, to evaluate their reduced width amplitudes and spectroscopic factors, using Eqs. (4.12)–(4.14) with $u_l(r)$ replacing $\phi_l(r)$ in Eq. (4.12). In these calcula-

tions the depth parameter of Eq. (4.1) was fixed to the value $V_0 = 180$ MeV. The results of this expansion are presented pictorially in Fig. 3 for a few representative cases, together with the corresponding wave functions and reduced width amplitudes; the wave functions are compared with the HO wave functions with quantum numbers corresponding to the $(\lambda,\mu) = (12,0)$ SU(3) limit, i.e., $(N,l) = (12,l)$. The values obtained for the spectroscopic factors are listed in Table III.

Whereas the SU(3) (12,0) component of the $J^\pi = 0^+$ wave function is seen to amount to only 50%, this proportion increases progressively with spin to reach 95% for the $J^\pi = 12^+$ state. This evolution within the band is paralleled by that of the spectroscopic factor which falls from 0.205 for the 0^+ state to 0.084 for the 12^+ state; these values should be compared with their SU(3) limit of 0.069. Even in the case of the 0^+ state, the strength is seen to be concentrated on a limited number of HO states. Examination of the wave functions likewise indicates that they do not extend considerably in the surface region with respect to their HO counterparts, corroborating the view, already expressed in connection with the examination of the rms radii, that the $N = 12$

TABLE III. Spectroscopic factors S_α calculated for the states of the $N = 12$ and $N = 13$ bands in ^{44}Ti.

J^π	S_α	J^π	S_α
0^+	0.20	1^-	0.42
2^+	0.20	3^-	0.41
4^+	0.18	5^-	0.38
6^+	0.16	7^-	0.34
8^+	0.13	9^-	0.29
10^+	0.11	11^-	0.23
12^+	0.08	13^-	0.19

band—and thus the ^{44}Ti ground state band which we associate with it—does not have a strong cluster character, and that the higher spin states are nearly pure shell-model states (this could explain why the energy location of the latter is badly described in the simple local potential picture). It has to be stressed again, however, that even a modest amount of cluster components in the wave functions proves instrumental in enhancing the electromagnetic transition rates, as has been illustrated by Tomoda and Arima[3] in the case of ^{20}Ne.

B. The excited positive-parity band

In addition to the ground state band, the potential supports an excited $N = 14$ positive-parity band located well above the threshold. These states are displayed in Fig. 1(b) together with those of the g.s. band and additional states to be discussed later; the theoretical energies were calculated using the average potential depth $V_0 = 180$ MeV.

The $N = 14$ excited band is composed of states located near the top of their respective effective potential barriers, and have therefore rather large widths of the order of 1 MeV. The corresponding reduced widths[48,50] γ_l^2 can in principle be deduced from the reduced width amplitude $y_l(r)$ of Eq. (4.13) evaluated at some conveniently chosen channel radius a; they are given by

$$\gamma_l^2 = \frac{\hbar^2}{2\mu a} y_l^2(a) . \tag{4.15}$$

The dimensionless reduced width θ_l^2 defined as the ratio of γ_l^2 to the Wigner limit reads

$$\theta_l^2 = \frac{2\mu a^2}{3\hbar^2} \gamma_l^2 . \tag{4.16}$$

On the other hand, γ_l^2 can directly be deduced from the total width Γ_l from

$$\Gamma_l = 2P_l \gamma_l^2 , \tag{4.17}$$

where P_l denotes the penetration factor estimated at the channel radius, which is expressed in terms of the usual Coulomb wave functions F_l and G_l. The total width Γ_l itself can be extracted from the energy behavior of the phase shift as

$$\Gamma_l = 2/(d\delta_l/dE)_{E=E_r} \tag{4.18}$$

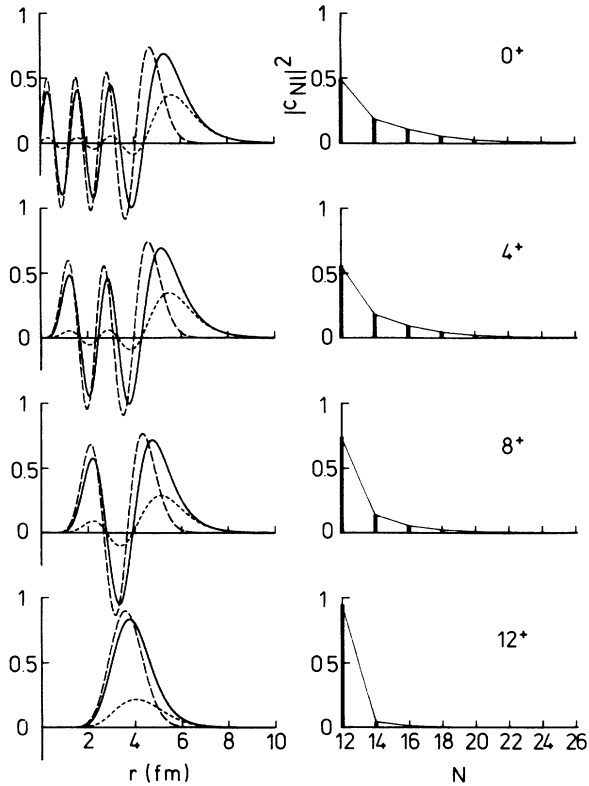evaluated at the resonance energy E_r (defined as the en-

FIG. 3. Normalized wave functions $u_l(r)$ (full line), reduced width amplitudes $y_l(r)$ (short-dashed line), and harmonic oscillator wave functions $u_{N=12,l}^{HO}(r)$ (long-dashed line) for the $J^\pi = 0^+$, 4^+, 8^+, and 12^+ states of the $N = 12$ band calculated with the local potential with $V_0 = 180$ MeV (left-hand side). Square of the expansion coefficients of the wave functions of the same states in the harmonic oscillator basis with $\nu' = 0.509$ fm^{-2} as a function of N (right-hand side).

ergy where the phase shift crosses $\pi/2$ up to a constant multiple of π). The very detailed study of Arima and Yoshida[51] has revealed that formula (4.17) gives estimates of the total width which are stable as a function of the channel radius only for narrow resonances; for broad resonances it has to be generalized to

$$\Gamma_l = 2 \Big/ \left[\frac{\overline{G}_l^{\,2}}{ka} \left[\frac{1}{\gamma_l^2} + \dot{\overline{S}} - \dot{\overline{P}} \frac{\overline{F}_l}{\overline{G}_l} \right] - \dot{\overline{\phi}} \right], \qquad (4.19)$$

where $\overline{S}$ and $\overline{\phi}$ represent the usual shift function and hard sphere phase shift of standard R-matrix theory,[50] and the overdots denote energy derivatives. Formula (4.19) reduces to Eq. (4.17) for narrow resonances; it predicts total widths Γ_l which do not depend on the channel radius, provided the pure Coulomb wave functions F_l and G_l are replaced by modified Coulomb wave functions $\overline{F}_l$ and $\overline{G}_l$ in the evaluation of P, S, and ϕ ($\overline{F}_l$ and $\overline{G}_l$ are defined as satisfying the full Schrödinger equation including the nuclear term, and they have the same asymptotic behavior as their pure Coulomb counterparts).

In the following, the choice of a channel radius $a = 7.5$ fm was made, scaling the values $a \cong 5-6$ fm often used in the much studied ^{20}Ne case[2] according to an $A^{1/3}$ prescription. It was checked in the case of narrow and medium width resonances to be discussed below, where reduced width amplitudes are readily available that estimating the reduced width γ_l^2 through Eq. (4.15) or through Eqs. (4.18) and (4.19) leads to nearly identical results. For broader resonances like those of the $N = 14$ band we are considering here, it is difficult to obtain properly normalized relative motion wave functions $u_l(r)$, and hence convenient reduced width amplitudes $y_l(r)$, because these states can no more be treated meaningfully in the bound state approximation. In that case we restricted ourselves to the use of Eqs. (4.18) and (4.19) to derive the reduced widths γ_l^2 and θ_l^2 from the phase shift energy behavior.

The extracted reduced widths as well as the total widths and resonance energies of the states of the $N = 14$ band are reported in Table IV. The total widths of the first five states are seen to be of comparable magnitude $\Gamma \sim 1$ MeV, while they become smaller for the last

TABLE IV. Resonance energies and widths of the members of the ^{44}Ti $N = 14$ excited positive parity band, together with the corresponding dimensionless reduced widths θ_l^2 calculated with a channel radius $a = 7.5$ fm.

J^π	$E_{r,\text{c.m.}}$ (MeV)	E_x (MeV)	$\Gamma_{\text{c.m.}}$ (MeV)	θ_l^2 (%)
0^+	6.6	11.7	1.10	122
2^+	7.1	12.3	1.15	112
4^+	8.4	13.6	1.20	97
6^+	10.4	15.5	1.13	78
8^+	13.1	18.2	0.91	55
10^+	16.6	21.7	0.59	32
12^+	20.8	26.0	0.25	12
14^+	25.7	30.8	0.05	2

members of the band. The reduced widths, which are of the order of the Wigner limit for the first states, correspondingly become very small for the $J^\pi = 12^+$ and 14^+ states. It has to be remarked that the last states of the band are predicted to lie at an appreciable excitation energy, where coupling with other channels could lead to observable widths differing somewhat from the real potential estimates of Table IV. In particular, the growing importance of absorption is likely to make these states completely unobservable in the elastic channel. Also, the predictions could be sensitive to the exact energy location of the states with respect to the effective potential barriers.

The correctness of the energy location of the predicted states with respect to the threshold has, however, recently received an independent confirmation from a study of the present authors[41] of the experimental $\alpha + {}^{40}$Ca fusion excitation function of Eberhard et al.[52] between 10 and 27 MeV. Indeed we showed in that work that the broad oscillations observed in the data could be ascribed to the $J^\pi = 6^+$ to 12^+ members of the $N = 14$ band, and that the location and width of the experimental structures could be described within a simple fusion model using the same real potential as here with $V_0 = 180$ MeV.

The contribution of the low spin states of the band ($J^\pi = 0^+$ to 4^+) is predicted to lie outside the range spanned by the fusion data. However, the calculation locates the first two members at excitation energies very close to those of the broad experimental positive parity states observed in elastic scattering[10] with $J^\pi = 0^+$, $E_x = 11.2$ MeV and $J^\pi = 2^+$, $E_x = 12.2$ MeV. A closer examination of these states reveals that they can be considered as strong candidates for the band head of the $N = 14$ band. In fact, the extraction of their dimensionless reduced widths from the experimental total widths, using the same channel radius $a = 7.5$ fm as above, leads to $\theta_0^2 = 117\%$ and $\theta_2^2 = 30\%$; the first value is in excellent agreement with our predictions, while the second one is somewhat too low (see Table IV).

As pointed out above, it is difficult to calculate reduced width amplitudes, spectroscopic factors, and rms radii for states as broad as those considered here. However, examination of the relative motion wave functions shows that they extend considerably further out than those of the states of the ground state band. This is displayed in Fig. 4 where we compare the wave functions of the lowest spin states of the band with their $(\lambda,\mu) = (14,0)$ SU(3) limit. The much stronger cluster character of these states (at least at low spin) is confirmed by the proximity of the reduced widths to their Wigner limit. The $N = 14$ band thus appears to be the exact analog of the well-known "higher nodal" $N = 10$ band built on the $J^\pi = 0_4^+$, $E_x \cong 8.3$ MeV state in ^{20}Ne.

We end this subsection by examining the status of the narrow $J^\pi = 1^-$, $E_x = 11.7$ MeV state found by Frekers et al.[8,10] in their analysis of high resolution ^{40}Ca(α,α_0) excitation function and postulated to belong to a mixed-parity rotational band with the 0^+ and 2^+ states we have just discussed as band partners. (A $J^\pi = 3^-$ state with $\Gamma = 220$ keV was extracted by the same group[10] at

$E_x = 12.8$ MeV, but its spin determination is far less conclusive and should be confirmed independently.) The interpretation of this state as a simple $\alpha + ^{40}$Ca (g.s.) cluster state not only disagrees with the present picture, but it is untenable because of the incompatibility of its very small width ($\Gamma = 40$ keV) with its position with respect to the $l = 1$ barrier. Indeed the calculation of its reduced width (using the channel radius $a = 7.5$ fm) leads to $\theta_1^2 = 4.4\%$, to be compared with the value $\theta_0^2 = 117\%$ found for the $J^\pi = 0^+$, $E_x = 11.2$ MeV state (for the tentative 3^- state at 12.8 MeV, we likewise find $\theta_3^2 = 19\%$). [Note that the large reduced width sometimes quoted for this state results from the choice of an unrealistically small value of the channel radius and the use of the simple formula (4.17) with pure Coulomb wave functions. For example, in Ref. 12 use is made of a channel radius of 5.5 fm, which leads to a dimensionless reduced width for this state of some 40%; however, at $r = 5.5$ fm the nuclear interaction is far from being negligible, as with our potential it amounts to more than 20 MeV. At the channel radius of 7.5 fm chosen here it has dropped to less than 2 MeV.] On the other hand, the GCM calculation of Langanke,[14] which is used to support the interpretation of this mixed-parity rotational band, leads to
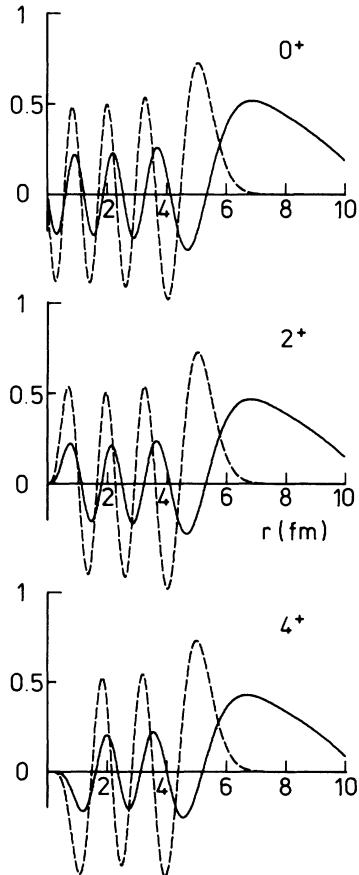

FIG. 4. Comparison of the relative motion wave functions of the first members of the $N = 14$ band (full line) calculated in the local potential, with the harmonic oscillator wave functions $u_{N=14,l}^{HO}(r)$ (long-dashed line) (the wave function normalization is arbitrary).

$\theta_1^2 = 93\%$ and $\theta_3^2 = 91\%$ (for the 0^+ and 2^+ states of the same calculation one finds $\theta_0^2 = 62\%$ and $\theta_2^2 = 69\%$). Although the spin determination of the $J^\pi = 1^-$, $E_x = 11.7$ MeV state seems to be unambiguous, the very small value of its reduced width with respect to the Wigner limit—and with respect to that of the neighboring 0^+ and 2^+ states—clearly demonstrates that this state does not have the same simple structure of an unexcited-core cluster state.

C. The $N = 13$ negative-parity band

The calculation invariably locates a $N = 13$ negative-parity band halfway between the $N = 12$ and the $N = 14$ positive-parity bands; its band head is predicted to lie slightly above the $\alpha + ^{40}$Ca threshold (see Fig. 1). As these states fall considerably below their respective effective potential barriers they are much narrower than those of the $N = 14$ band and their wave functions can be calculated within the bound state approximation.

We have also calculated the $B(E2)$ intraband transition rates for the states of this band using the average potential depth of 180 MeV; these are listed in Table V, together with the corresponding rms radii. Both the stronger $B(E2)$'s and larger rms radii, as compared with those of the ground state band, indicate that the $N = 13$ band has a stronger cluster character than the latter. Also, examination of the evolution of the rms radii within the band reveals a strong antistretching effect which reduces significantly this cluster character for the high spin members of the band.

To give more quantitative support to these remarks, we also expanded the local potential wave functions of the states of the $N = 13$ band in the HO basis with $\nu' = 0.509$ fm^{-2}, and evaluated their reduced width amplitudes and spectroscopic factors (see Sec. IV A). The results of these calculations are presented for a few of these states in Fig. 5, together with the HO wave functions corresponding to the $(\lambda, \mu) = (13, 0)$ SU(3) limit, the spectroscopic factors appearing in Table III. Whereas the strength of the members of the ground state band were found to be concentrated on the first few HO components, it is seen to be more widely scattered here for the first members of the band: the SU(3) $(\lambda, \mu) = (13, 0)$ component of the 1^- state amounts to only 20%. The spectroscopic factor is correspondingly enhanced, reaching a value of 0.42 for the same state (to be compared with the SU(3) limit of 0.157). At the other end of the

TABLE V. Calculated rms radii and quadrupole transition probabilities for the states of the ^{44}Ti $N = 13$ band.

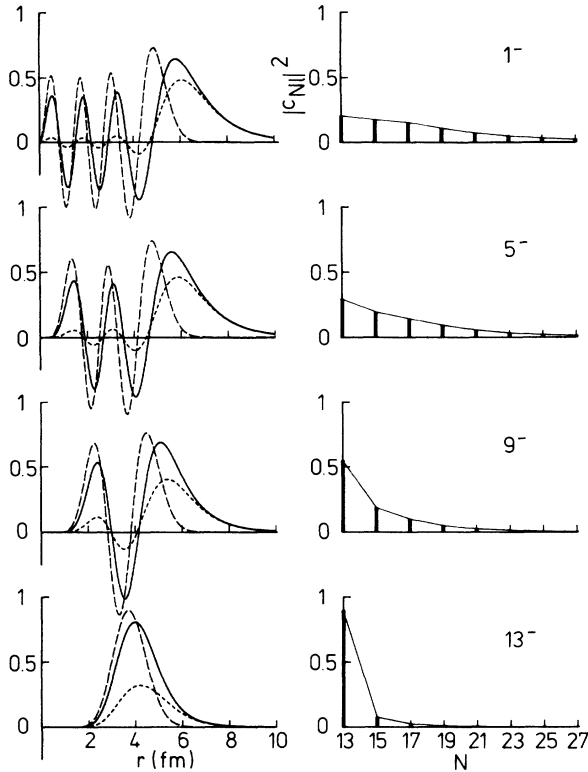| J^π	$\langle R^2 \rangle^{1/2}$ (fm)	$B(E2)$ $(J \rightarrow J - 2)$ $(e^2 \text{fm}^4)$
1^-	5.35	
3^-	5.28	264.7
5^-	5.15	279.1
7^-	4.95	243.6
9^-	4.71	184.5
11^-	4.43	118.1
13^-	4.14	54.9

FIG. 5. Same as Fig. 3 for the $J^\pi = 1^-$, 5^-, 9^-, and 13^- members of the $N = 13$ band.

band, the (13,0) component of the 13^- state has increased to 89%, while S_α has dropped to a value not far from the SU(3) limit, again pointing out the progressive loss of the cluster character of the states with increasing spin.

Finally, we calculated the total and reduced widths of these states (using a channel radius $a = 7.5$ fm); the resonance energies and widths are listed in Table VI. It is seen that these states are expected to have exceedingly small widths ranging from a few eV's to about 1 keV; again the exact location of these states could alter these estimates significantly. The dimensionless reduced widths, on the other hand, are an appreciable fraction of the Wigner limit at the beginning of the band but they drop to very small values at high spin. Even for the first

TABLE VI. Resonance energies and widths of the members of the ^{44}Ti $N = 13$ negative parity band, together with the corresponding dimensionless reduced widths θ_l^2 calculated with the channel radius $a = 7.5$ fm.

J^π	$E_{r,c.m.}$ (MeV)	E_x (MeV)	$\Gamma_{c.m.}$ (keV)	θ_l^2 (%)
1^-	2.83	7.95	2.0×10^{-3}	16
3^-	3.63	8.75	33.5×10^{-3}	14
5^-	5.01	10.13	0.347	10
7^-	6.97	12.09	1.14	6.4
9^-	9.49	14.61	1.34	2.8
11^-	12.55	17.67	0.656	0.8
13^-	16.11	21.23	0.107	0.1

states they are nearly an order of magnitude smaller than those of the $N = 14$ states. The $N = 13$ band has thus an intermediate cluster character between that of the shell-model-like ground state band and the strongly clusterlike $N = 14$ positive-parity band. Its cluster character seems to be somewhat less than that of the "inversion doublet" $K^\pi = 0^-$ negative-parity band in ^{20}Ne,[2] of which it is the close analog.

Examination of Fig. 1 reveals no known experimental counterparts to the states of our $N = 13$ band. However, the theoretical band head is not far from the $J^\pi = (0^+)$, $E_x = 8.54$ MeV state extracted by Strohbusch et al.[7] from their ^{40}Ca(^{6}Li,d) transfer experiment; this very narrow level is strongly excited by (^{6}Li,d) transfer, and it is also copiously populated in the ^{40}Ca(^{16}O,^{12}C) reaction.[53] The spin of this state was suggested by comparison with the predictions of a standard distorted-wave Born approximation (DWBA) calculation; the analysis was, however, complicated by the fact that this state is located above the $\alpha + {}^{40}$Ca threshold, and therefore the spin deduced was only tentative. The level near $E_x = 6.03$ MeV, strongly excited in both (^{6}Li,d) and (^{16}O,^{12}C) transfer reactions,[7,53,54] can also be considered as a plausible band head. A few isolated states, located higher in energy, and strongly excited by (^{6}Li,d) transfer,[7] but lacking spin assignments, can also be considered as possible candidates for other low spin members of the band. Clearly additional experimental work is needed to clarify the situation. As the standard DWBA analysis often leads to ambiguities in the spin assignments, particularly at high excitation energy, the measurement of d-α angular correlations in the (^{6}Li,d) transfer reaction[55] can be considered as an interesting alternative for identifying the low spin states of the $N = 13$ band. Another possibility could be to locate directly these states in a resonance scattering experiment, as has recently been achieved by Mac Arthur et al.[33] for the $J^\pi = 1^-$, $E_x = 5.782$ MeV and $J^\pi = 3^-$, $E_x = 7.156$ MeV states of the $K^\pi = 0^-$ band in ^{20}Ne (in addition the same group succeeded in measuring the quadrupole transition rate between these two states). In the case of the ^{20}Ne $J^\pi = 1^-$ state the measured width amounts to only 28 eV, and the interference with pure Coulomb scattering at $\theta_{c.m.} = 160°$ does not exceed 5% of the Rutherford cross section.[33] In contrast, if we locate the $J^\pi = 1^-$ state of the $N = 13$ band in ^{44}Ti at the energy of the $E_x = 8.54$ MeV level of Strohbusch et al.[7] by slightly reducing our potential depth (a depth $V_0 = 177.7$ MeV is required for that purpose), its width shifts from 2 eV (cf. Table VI) to about 100 eV and the interference with Coulomb scattering is predicted to reach 100%. This is likely to be a delicate experiment, however, because of target thickness and energy resolution problems; if feasible it would be possible to decide unambiguously whether the spin of the resonance is 0 or 1 by a simple inspection of the $\theta_{c.m.} = 90°$ excitation function which should display no structure in the latter case.

D. Higher lying excited bands

Examination of the potential phase shifts (Fig. 6) indicates the existence at still higher energy of very broad

states belonging to incomplete bands with higher N values. The most conspicuous are the $J = 11$, 13, and 15 members of an $N = 15$ band, and the $J = 14$ and 16 members of an $N = 16$ band (lower spin members are lacking since the corresponding phase shifts hardly exceed $\pi/2$ or even display no resonant behavior at all). At higher energies genuine resonant contributions die away since the effective potential loses its inside "pocket" for $l > 17$, $E_\alpha \gtrsim 55$ MeV. As these states are very broad and overlapping their individual contributions cannot be isolated in the elastic scattering angular distributions and excitation functions, the more so as absorption has become comparatively important at these energies: it seems more adequate to view the scattering as dominated at each energy by those segments of the Regge pole trajectories associated with the potential which are nearest to the grazing angular momentum value L_{gr} at that energy[56] (we define L_{gr} as the particular angular momentum for which the top of the effective potential barrier is equal to the incident energy). As a result the backward angular distribution behaves approximately as the square of a Legendre polynomial of order L close to L_{gr} increasing with energy as $E^{1/2}$; plotting the energies where fits of Legendre polynomials are performed at backward angles as a function of $L(L + 1)$ therefore automatically results in a quasirotational sequence. This mechanism produces a regular succession
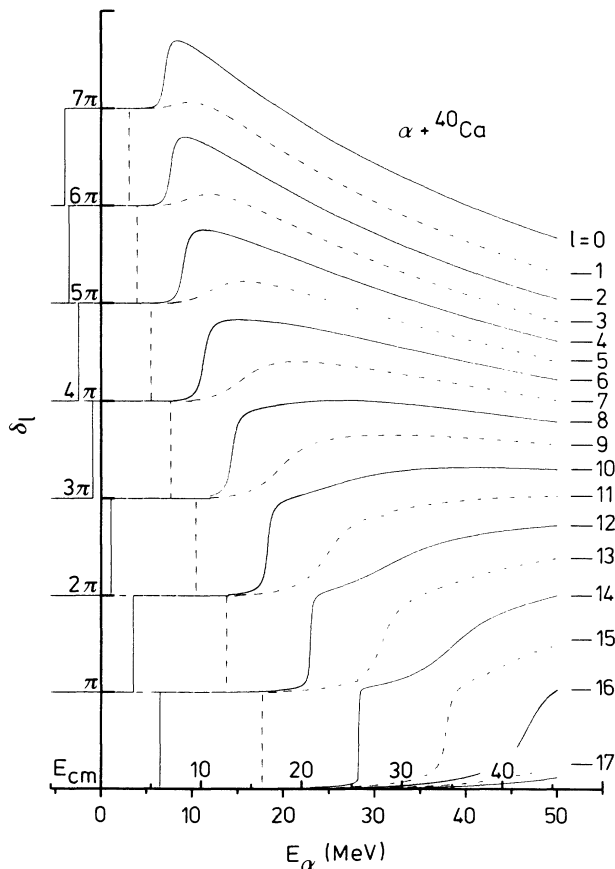
of alternating odd and even P_l^2 backangle behaviors, whereas the underlying rotational bands are in essence split in parity. However, it would be misleading[30,57] to deduce from this plot, as was the case in early rotator interpretations of anomalous large angle scattering,[58] the existence of a single rotational band, since the grazing angular momentum trajectory in the $(E, J(J + 1))$ plane crosses several of the bands (labeled by principal quantum numbers $N = 2n_r + l$ ranging from 14 to 16) supported by the potential. Similarly, the particular Regge trajectory which dominates the scattering at a given energy, which can be labeled by the radial quantum number n_r, changes with increasing energy. This crossing of the various Regge trajectories has recently been shown[56,59] to be responsible for the very broad oscillations observed in the elastic scattering backward angle excitation function above 20 MeV incident energy (which alternatively can be viewed in terms of a barrier-wave–internal-wave interference effect[60]). These findings are in line with the very recent investigation by Ohkubo[61] of the mechanism of the backward angle enhancement.

V. SUMMARY AND CONCLUSIONS

A rather clear-cut and unambiguous picture of the ^{44}Ti α-cluster spectroscopy is seen to emerge from the present study, whose findings are briefly summarized here.

Starting from the unique optical potential describing ^{40}Ca(α, α_0) scattering from low $(E_\alpha \cong 10$ MeV) to high $(E_\alpha = 166$ MeV) incident energies, as well as the $\alpha + {}^{40}$Ca fusion data between 10 and 27 MeV, we were able to enumerate and classify the various $\alpha + {}^{40}$Ca (g.s.) cluster bands of the ^{44}Ti nucleus. Although there exist quantitative differences with respect to the archetypal case of ^{20}Ne, the ^{44}Ti cluster properties are not dissimilar to those of the latter nucleus. Indeed its ground state (positive parity) band is composed of states whose cluster character, which is moderate at low spin, becomes very small near the end of the band as the corresponding relative motion wave functions become nearly identical to their simple SU(3) limit there. This decrease of the cluster character is testified by the evolution of the rms radii and spectroscopic factors within the band. However, these rather modest cluster admixtures have been shown to be instrumental for a correct description of the intraband quadrupole transition probabilities without having to introduce unrealistically large effective charges as is needed in shell-model calculations.

The potential supports, in addition, an excited positive parity band, with spins ranging from 0 to 14, starting a few MeV's above the $\alpha + {}^{40}$Ca threshold, whose low spin states have total widths of the order of 1 MeV and reduced widths close to their Wigner limits; this band is the close analog of the well-known "higher nodal" $K^\pi = 0_4^+$ band of ^{20}Ne. States of this band with spins ranging from 6 to 12 have recently been shown to be responsible for the broad oscillations seen in the experimental $\alpha + {}^{40}$Ca fusion excitation function between 10 and 27 MeV. The first two members of this band nearly coincide in energy with the broad experimental $J^\pi = 0^+$, $E_x = 11.2$ MeV and $J^\pi = 2^+$, $E_x = 12.2$ MeV levels ob-

FIG. 6. Absolute phase shifts and bound states calculated with the local potential ($V_0 = 180$ MeV).

served by Frekers et al.[10] in their high resolution elastic scattering excitation functions, which we consider as serious candidates for the head of this band.

Halfway between these two positive parity bands the potential inevitably predicts the existence of a negative parity band starting just above the threshold. The cluster character of the states of this band is found to be intermediate between that of the two above-mentioned positive parity bands; as the ground state band, it displays a strong antistretching effect which reduces the cluster character of its high spin members. The analog of this band in ^{20}Ne is the "inversion doublet" $K^{\pi}=0^-$ band built on the $J^{\pi}=1^-$, $E_x=5.782$ MeV state. Although there is up to now no known experimental counterpart to this band, we have raised the possibility that the $J^{\pi}=(0^+)$, $E_x=8.54$ MeV state seen by Strohbusch et al.[7] in their ^{40}Ca(^{6}Li,d) transfer experiment could have spin 1 and therefore provide the missing band head.

Higher lying excited bands predicted by the potential are incomplete and composed of very broad, overlapping states; the members of these bands, although not identifiable individually in the elastic scattering data, play an important role in enhancing the backward angle cross section, causing the spectacular anomalous large angle scattering that initiated interest for the $\alpha+^{40}$Ca system.

Although detailed agreement is lacking, the picture which emerges from the present work agrees best with the RGM calculations performed some ten years ago by Kihara et al.,[12] and also with the more recent hybrid calculation of Itonaga;[18] in particular, both predict parity-split rotational bands and the existence of a negative parity band starting near the threshold. As these calculations predict somewhat larger moments of inertia for the calculated bands, correspondence with experiment is, however, established differently from here for the excited bands (see Sec. II): the band head of the second positive and negative parity bands predicted in these calculations are speculated to correspond to the experimental $J^{\pi}=(0^+)$, $E_x=8.54$ MeV and $J^{\pi}=1^-$, $E_x=11.7$ MeV levels. The recent calculation of Horiuchi[16] does not produce the first two bands, but the band heads of the first two (decoupled) positive and negative parity bands found in his calculation are also put in correspondence with the same experimental levels.

Our picture is in stronger disagreement with the calculations of the Münster group.[14] Indeed the latter predict the first band to start well above the threshold, and moreover this band is found to be of mixed parity, at least at low spin. The first states of the band have been put in correspondence with levels found in an elastic scattering experiment specifically designed in view of their identification.[10] However, as was discussed in Sec. IV B, the strong dissimilarity of the widths of the positive and negative parity levels extracted in this experiment precludes their interpretation as members of a common unexcited-core cluster band, despite the specific coupling mechanisms which were invoked in Ref. 10 to explain this dissymmetry. Moreover, the ambiguities inherent to this type of analysis of strongly fluctuating

data make the spin determination of all but the very low spin states very difficult, so that an independent determination of these spins would be highly desirable.

The links of our picture with that emerging from the microscopic calculations of the Münster group can usefully be discussed in terms of the local potential description. Indeed Wintgen et al.[22] have built local equivalent potentials reproducing the results of the full microscopic calculation starting from the angular momentum projected energy curves of the GCM; these potentials are energy independent but somewhat l dependent, and they can be expressed in analytical form in terms of a small number of parameters. Although these potentials are designed to be plugged into an OCM equation [cf. Eq. (4.4)], it is sensible to compare them directly with our local potential since the scattering states of the latter are automatically orthogonal to those of the bound states which simulate (with good accuracy, as was shown above) the forbidden states of the RGM. We have calculated the first moments of these potentials; the volume integrals per nucleon pair $J_v/4A$ are found to vary between 260 and 320 MeV fm^3, while the rms radii $\langle r^2 \rangle^{1/2}$ assume values between 4.40 and 4.50 fm. These values are significantly different from those calculated form the empirical potentials belonging to the unique potential family; although the latter show some model dependence and vary slowly with incident energy, they are better determined than the potential itself, and assume values of about 350 MeV fm^3 and 4.25 fm at low energy, respec-
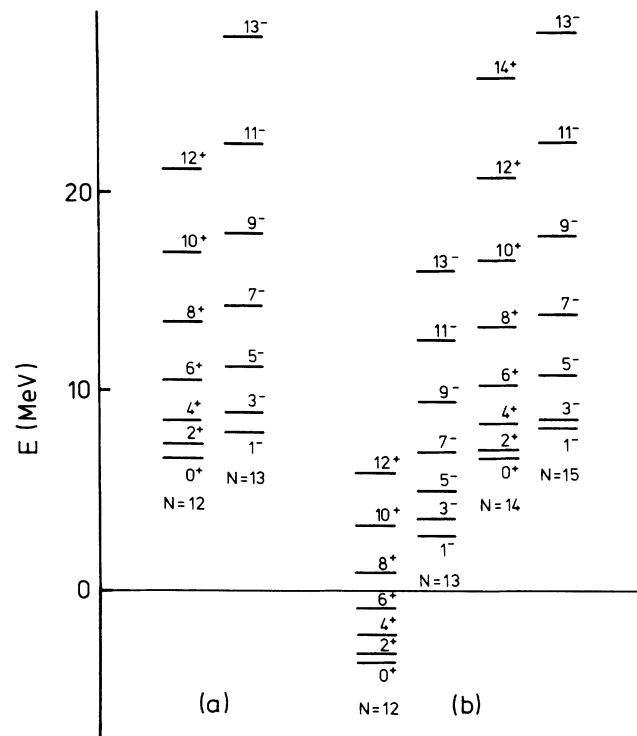

FIG. 7. Comparison of the band structure predicted by (a) potential No. 1 of Gubler et al. (Ref. 40, p. 35) and (b) our local potential with $V_0=180$ MeV.

tively.[29,39,40] The values of the volume integrals and rms radii of the local potentials of the Münster group agree in fact much better with those of the empirical potentials belonging to the shallower potential family, whose wave functions admit one internal node less than those generated by potentials of the correct family: for these shallower potentials one has indeed $J_v/4A \cong 280$ MeV fm^3 and $\langle r^2 \rangle^{1/2} \cong 4.45$ fm.[40] As a result the spectrum obtained by this group is very similar to that generated by potentials of the shallower family. A comparison of the physical spectra calculated with potential No. 1 of Gubler et al. (see Ref. 40, p. 35), which has $J_v/4A = 279$ MeV fm^3 and belongs to that family, and with the present potential (using $V_0 = 180$ MeV) appears in Fig. 7. The energy locations of the states common to these two potentials are found to be nearly identical; however, the band which we have put in correspondence with the ^{44}Ti ground state band and the first negative parity band of our potential are missing in Gubler No. 1 potential, and the nature of the higher lying bands is different, as their principal quantum numbers differ by two units. The ending of these bands at different angular momenta makes the rainbow scattering regime appear at too low an energy with Gubler No. 1 potential, which therefore is ruled out by experiment. Note that the (small) parity splitting between the first two bands of the Gubler potential can be suppressed by introducing a weak parity dependence in the potential, and indeed the local equivalent potentials of the Münster group, which predict no splitting at low spin, display such a dependence. However, we recall that the parity splitting of these two bands was found necessary for a correct reproduction of the low energy fusion oscillations.[41]

The microscopic calculations of the Münster group were carried out using the Brink and Boeker interaction[15] $B1$ without changing any of its parameters. For lighter systems where part of the spectrum is well established, it has been of constant practice to use effective interactions where some parameter is tuned to locate correctly these states with respect to the threshold; one of the most popular is the $V(1$ or $2)$ Volkov interaction,[13] where the Majorana exchange parameter m (or

sometimes the depth parameter) is used as an adjustable parameter. It is well known that in the mass region considered here the Brink and Boeker interaction used as it is tends to underbind nuclei (in contrast with the Volkov interaction which, with its original parameters, has overbinding properties). This deficiency is not restricted to the absolute energy of the unified system, but it affects also the evaluation of the separation energy of the partners; for example for the ^{20}Ne system, the original $B1$ interaction predicts too weak binding with respect to the $\alpha + {}^{16}$O channel, the ^{20}Ne ground state being located above the threshold.[62] It is thus not surprising that the same situation is found for the $\alpha + {}^{40}$Ca system.

The most stringent test of the correctness of our picture is undoubtedly the presence of a negative parity band starting just above the $\alpha + {}^{40}$Ca threshold, whose low spin members should display appreciable cluster character. The first states of this band should be actively searched for; the measurement of d-α correlations in the $(^6$Li,d$)$ transfer reaction, which has been so efficient in the sd shell,[55] could make possible the identification and unambiguous spin determination of these states. Alternatively, a very high resolution experiment could possibly allow a direct detection of these states through elastic scattering excitation function measurements.

ACKNOWLEDGMENTS

[1]D. A. Bromley, in Proceedings of the Fourth International Conference on Clustering Aspects of Nuclear Structure and Nuclear Reactions, Chester, United Kingdom, edited by J. S. Lilley and M. A. Nagarajan (Reidel, Dordrecht, 1985), p. 1.

[2]See, e.g., Y. Fujiwara, H. Horiuchi, K. Ikeda, M. Kamimura, K. Kato, Y. Suzuki, and E. Uegaki, Suppl. Prog. Theor. Phys. 68, 29 (1980), and references therein.

[3]T. Tomoda and A. Arima, Nucl. Phys. A303, 217 (1978).

[4]See, e.g., H. Furutani, H. Kanada, T. Kaneko, S. Nagata, H. Nishioka, S. Okabe, S. Saito, T. Sakuda, and M. Seya, Suppl. Prog. Theor. Phys. 68, 193 (1980), and references therein.

[5]F. Michel, G. Reidemeister, and S. Ohkubo, Phys. Rev. Lett. 57, 1215 (1986).

[6]Table of Isotopes, edited by C. M. Lederer and V. S. Shirley (Wiley, New York, 1978).

[7]U. Strohbusch, C. L. Fink, B. Zeidman, R. G. Markham, H. W. Fulbright, and R. N. Horoshko, Phys. Rev. C 9, 965 (1974).

[8]D. Frekers, H. Eickhoff, H. Löhner, K. Poppensieker, R. Santo, and C. Wiezorek, Z. Phys. A 276, 317 (1976).

[9]J. John, C. P. Robinson, J. P. Aldridge, and R. H. Davis, Phys. Rev. 177, 1755 (1969).

[10]D. Frekers, R. Santo, and K. Langanke, Nucl. Phys. A394, 189 (1983).

[11]A. Chatterjee, S. Kailas, S. Saini, S. K. Gupta, and M. K. Mehta, Z. Phys. A 317, 209 (1984).

[12]H. Kihara, M. Kamimura, and A. Tohsaki-Suzuki, in Proceedings of the International Conference on Nuclear Structure, Tokyo, 1977, edited by the Organizing Committee (International Printing Co. Ltd., Tokyo, 1977), p. 235.

[13]A. B. Volkov, Nucl. Phys. 74, 33 (1965).

[14]H. Friedrich and K. Langanke, Nucl. Phys. A252, 47 (1975);

K. Langanke, *ibid.* A377, 53 (1982); K. Langanke and H. Friedrich, *Advances in Nuclear Physics,* edited by J. W. Negele and E. Vogt (Plenum, New York, 1986), Vol. 17, p. 223.

[15]D. M. Brink and E. Boeker, Nucl. Phys. A91, 1 (1967).

[16]H. Horiuchi, Prog. Theor. Phys. 73, 1172 (1985).

[17]K. H. Bhatt and J. B. Mc Grory, Phys. Rev. C 3, 2293 (1971); A. Poves and A. Zuker, Phys. Rep. 70, 235 (1981).

[18]T. Motoba and K. Itonaga, Suppl. Prog. Theor. Phys. 65, 136 (1979); K. Itonaga, Prog. Theor. Phys. 66, 2103 (1981).

[19]A. Arima, in *Proceedings of the Conference on Clustering Aspects of Nuclear Structure and Nuclear Reactions, Winnipeg, 1978,* edited by W. T. H. Van Oers, J. P. Svenne, J. S. C. McKee, and W. R. Falk (AIP, New York, 1978), p. 1.

[20]B. Buck, C. B. Dover, and J. P. Vary, Phys. Rev. C 11, 1803 (1975); B. Buck, H. Friedrich, and C. Wheatley, Nucl. Phys. A275, 246 (1977); B. Buck, in Ref. 1, p. 71.

[21]H. Horiuchi, in Ref. 1, p. 35, and references therein.

[22]H. Friedrich, Phys. Rep. 74, 209 (1981); D. Wintgen, H. Friedrich, and K. Langanke, Nucl. Phys. A408, 239 (1983).

[23]R. A. Baldock, B. A. Robson, and R. F. Barrett, Nucl. Phys. A366, 270 (1981).

[24]R. Lipperheide, H. Fiedeldey, E. W. Schmid, and S. A. Sofianos, Z. Phys. A 320, 265 (1985).

[25]H. Horiuchi, Prog. Theor. Phys. 69, 886 (1983).

[26]A. A. Pilt, Phys. Lett. 73B, 274 (1978).

[27]K. F. Pal and R. G. Lovas, Phys. Lett. 96B, 19 (1980).

[28]A. C. Merchant, J. Phys. G 10, 885 (1984).

[29]Th. Delbar, Gh. Grégoire, G. Paic, R. Ceuleneer, F. Michel, R. Vanderpoorten, A. Budzanowski, H. Dabrowski, L. Freindl, K. Grotowski, S. Micek, R. Planeta, A. Strzalkowski, and K. A. Eberhard, Phys. Rev. C 18, 1237 (1978).

[30]F. Michel, J. Albinski, P. Belery, Th. Delbar, Gh. Grégoire, B. Tasiaux, and G. Reidemeister, Phys. Rev. C 28, 1904 (1983).

[31]D. A. Goldberg and S. M. Smith, Phys. Rev. Lett. 29, 500 (1972).

[32]F. Ajzenberg-Selove, Nucl. Phys. A392, 1 (1983).

[33]J. D. Mac Arthur, H. C. Evans, J. R. Leslie, and H.-B. Mak, Phys. Rev. C 22, 356 (1980).

[34]T. Wada and H. Horiuchi, Phys. Rev. Lett. 58, 2190 (1987).

[35]S. Gamba, G. Ricco, and G. Rottigni, Nucl. Phys. A213, 383 (1973); M. M. Giannini and G. Ricco, Ann. Phys. (N.Y.) 102, 458 (1976).

[36]C. Mahaux and R. Sartor, Phys. Rev. Lett. 57, 3015 (1986).

[37]F. Michel and R. Vanderpoorten, Phys. Rev. C 16, 142 (1977).

[38]H. P. Gubler, U. Kiebele, H. O. Meyer, G. R. Plattner, and I. Sick, Phys. Lett. 74B, 202 (1978).

[39]F. Michel and R. Vanderpoorten, Phys. Lett. 82B, 183 (1979).

[40]H. P. Gubler, U. Kiebele, H. O. Meyer, G. R. Plattner, and I. Sick, Nucl. Phys. A351, 29 (1981).

[41]F. Michel, G. Reidemeister, and S. Ohkubo, Phys. Rev. C 34, 1248 (1986).

[42]K. Aoki and H. Horiuchi, Prog. Theor. Phys. 68, 2028 (1982).

[43]C. Mahaux, H. Ngô, and G. R. Satchler, Nucl. Phys. A449, 354 (1986); A456, 134 (1986).

[44]R. Ceuleneer, F. Michel, and G. Reidemeister, in *Proceedings of the Symposium on Resonances in Heavy-Ion Reactions,* edited by K. A. Eberhard (Springer, Berlin, 1982).

[45]J. J. Simpson, W. Dünnweber, J. P. Wurm, P. W. Green, J. A. Kuehner, W. R. Dixon, and R. S. Storey, Phys. Rev. C 12, 468 (1975); J. Britz, A. Chevallier, J. Chevallier, and B. Haas, Nucl. Phys. A262, 189 (1976).

[46]R. C. Barrett and D. F. Jackson, *Nuclear Sizes and Structure* (Clarendon, Oxford, 1977).

[47]S. Saito, Prog. Theor. Phys. 41, 705 (1969).

[48]H. Horiuchi and Y. Suzuki, Prog. Theor. Phys. 49, 1974 (1973).

[49]A. Arima, in *Heavy Ion Collisions,* edited by R. Bock (North-Holland, Amsterdam, 1979), Vol. 1, p. 417.

[50]A. M. Lane and R. G. Thomas, Rev. Mod. Phys. 30, 257 (1958).

[51]A. Arima and S. Yoshida, Nucl. Phys. A219, 475 (1974).

[52]K. A. Eberhard, Ch. Appel, R. Bangert, L. Cleeman, J. Eberth, and V. Zobel, Phys. Rev. C 43, 107 (1979).

[53]J. R. Erskine, W. Henning, and L. R. Greenwood, Phys. Lett. 47B, 335 (1973).

[54]H. W. Fulbright, C. L. Bennett, R. A. Lindgren, R. G. Markham, S. C. Mc Guire, G. C. Morrison, U. Strohbusch, and J. Toke, Nucl. Phys. A284, 329 (1977).

[55]K. P. Artemov, V. Z. Gol'dberg, I. P. Petrov, V. P. Rudakov, I. N. Serikov, and V. A. Timofeev, Yad. Fiz. 36, 1345 (1982) [Sov. J. Nucl. Phys. 36, 779 (1982)]; K. P. Artemov, V. Z. Gol'dberg, M. S. Golovkov, B. G. Novatskii, I. P. Petrov, V. P. Rudakov, I. N. Serikov, and V. A. Timofeev, Yad. Fiz. 37, 1351 (1983) [Sov. J. Nucl. Phys. 37, 805 (1983)]; A. Cunsolo, A. Foti, G. Immé, G. Pappalardo, G. Raciti, and N. Saunier, Phys. Lett. 112B, 121 (1982); W. D. M. Rae, in Ref. 1, p. 261.

[56]R. Anni and L. Taffara, Nuovo Cimento 79A, 159 (1984).

[57]S. Ohkubo, Y. Kondo, and S. Nagata, Prog. Theor. Phys. 57, 82 (1977).

[58]R. Stock, G. Gaul, R. Santo, M. Bernas, B. Harvey, D. Hendrie, J. Mahoney, J. Sherman, J. Steyaert, and M. Zisman, Phys. Rev. C 6, 1226 (1972).

[59]K. W. Mc Voy, Nucl. Phys. A455, 141 (1986).

[60]D. M. Brink and N. Takigawa, Nucl. Phys. A279, 159 (1977); S. Y. Lee, N. Takigawa, and C. Marty, *ibid.* A308, 161 (1978).

[61]S. Ohkubo, Phys. Rev. C 36, 551 (1987).

[62]D. M. Brink, H. Friedrich, A. Weiguny, and C. W. Wong, Phys. Lett. 33B, 143 (1970).